Available online at www.sciencedirect.com
ScienceDirect
Forest Ecology and Management 243 (2007) 259–273
Forest Ecology and Management
www.elsevier.com/locate/foreco

Patterns of forest regrowth following clearcutting in western Oregon as determined from a Landsat time-series

Todd A. Schroeder [a,*], Warren B. Cohen [b], Zhiqiang Yang [a]

[a] Department of Forest Science, Forestry Sciences Laboratory, Oregon State University, Corvallis, OR 97331, United States
[b] Forestry Sciences Laboratory, Pacific Northwest Research Station, USDA Forest Service, 3200 SW Jefferson Way, Corvallis, OR 97331, United States

Received 26 July 2006; received in revised form 15 February 2007; accepted 12 March 2007

Abstract

The rate at which forest vegetation re-establishes dominance after clearcut harvesting can impact many ecological processes, such as erosion/sedimentation, nutrient and water cycling, carbon storage potential, wildlife habitat, and trophic interactions. Although knowing a forest stand's current state of succession is useful, a clearer understanding of the impact forest harvesting has on the aforementioned ecological processes can be achieved with a more dynamic characterization of the successional process. To more fully model the continuous nature of forest regrowth following clearcut harvesting we extrapolated percent tree cover data collected by the U.S. Forest Service Pacific Northwest Forest Inventory and Analysis program to a cross-normalized Landsat time-series using a date-invariant regression modeling approach. Using three periods of mapped clearcuts we extracted and classified the extrapolated percent tree cover data into four regrowth classes (little to no, slow, moderate and fast). These forest regrowth classes were used to develop frequency distributions describing the landscape patterns of postharvest forest recovery for two ecological provinces in western Oregon. The patterns of forest regrowth observed over the three clearcut periods indicated a much higher percentage of fast regrowth in the Coastal Range Province and a much higher percentage of little to no regrowth in the Western Cascade Province. For both ecological provinces we observed the propensity for faster regrowth on north facing aspects, shallow slopes and at low elevations. The forest regrowth classes and the frequency distributions indicated that a wide range of successional stages could be found in both ecological provinces 18 years after clearcutting. The extension of forest regrowth trajectories to the spectral space of Landsat provided an opportunity to use CART statistical analysis to more fully investigate the climatic and topographic drivers influencing the rate of postharvest forest regrowth. Based on the Kappa statistic, predictions from both CART models were in ''fair'' to ''moderate'' agreement with the test samples. Both classification trees yielded ecologically interpretable insights into the environmental attributes influencing forest regrowth rates after clearcutting. In both ecological provinces, elevation followed by potential relative radiation (PRR) explained the largest amount of variation in forest regrowth rates. To gauge the effectiveness of predicting more generalized postharvest forest regrowth rates we combined the four forest regrowth classes into two general ''fast'' and ''slow'' categories. Based on the Tau statistic, the CART models correctly classified 12% (CRP) and 26% (WCP) more combined test samples than classification of the four regrowth classes.
Published by Elsevier B.V.

Keywords: Tree cover estimation; Vegetation change trajectories; Forest succession; Forest inventory data; Landsat time-series

1. Introduction

There is growing evidence suggesting considerable variability in the rate at which trees re-establish dominance following stand-replacing harvest disturbance in the temperate forests of the Pacific Northwest. This variability in forest regrowth has been observed even among stands with similar abiotic conditions and management prescriptions (Nesje, 1996; Tappeiner et al., 1997; Sabol et al., 2002; Yang et al., 2005; O'Connell et al., 2007). Re-establishment of forest vegetation after harvest is important because it can influence many ecological processes, such as erosion/sedimentation, nutrient and water cycling, carbon storage potential, wildlife habitat, trophic interactions, and because of the economic value of conifer trees in the region.

Variability in the timing of tree re-establishment is one of the most widely studied phenomenons in forest ecology (Franklin et al., 2002). In western Oregon, ground surveys

* Corresponding author. Tel.: +1 541 758 7758.
E-mail address: todd.schroeder@oregonstate.edu (T.A. Schroeder).

0378-1127/$ – see front matter. Published by Elsevier B.V.
doi:10.1016/j.foreco.2007.03.019

(e.g., Tappeiner et al., 1997) and interpretation of high-resolution aerial photographs (Nesje, 1996; Yang et al., 2005) have been previously utilized to study tree re-establishment, both of which are time consuming and expensive. Ground surveys are critical in understanding the role of local site factors controlling tree re-establishment, however the number of stands analyzed is often fewer than required to statistically validate relationships between the abiotic and biotic factors influencing forest regrowth. Studies based on the interpretation of high-resolution aerial photographs are useful in that they help establish the spatial and temporal extent over which regrowth variability is occurring, but they do not readily permit explicit spatial modeling of the phenomenon (Nesje, 1996; Yang et al., 2005). We seek to overcome these limitations by scaling estimates derived by ground survey and airphoto interpretation to the greater landscape using Landsat data. This synergistic approach should effectively increase the number of stands available for statistical modeling, thus offering an opportunity to advance our understanding of the geographically referenced environmental attributes influencing rates of forest regrowth following clearcutting in western Oregon.

The use of satellite imagery to characterize forest successional processes has mainly focused on estimating forest age from single image dates to make inferences about successional stage condition at one point in time (Fiorella and Ripple, 1993; Peterson and Nilson, 1993; Jakubauskas, 1996; Cohen et al., 2001; Song et al., 2007). The difficulty with this approach is that the relationship between forest age and spectral data can be highly variable, especially for young (<20 year) stands with low canopy cover (Horler and Ahern, 1986). A more limited number of studies have taken advantage of multiple images to study the dynamic process of forest succession (Hall et al., 1991; Foody et al., 1996; Lucas et al., 2002), but have utilized relatively simple techniques such as post-classification comparison to estimate forest change. Although simple to execute, post-classification comparison relies on differencing two or more independently produced image classifications. Thus, its effectiveness at estimating forest change is hindered by the fact that errors inherent to each individual classification combine multiplicatively as they are overlaid for comparison, resulting in a final change product that contains more error than any of the original classification-based inputs.

An alternative use of satellite imagery for characterizing forest successional processes is through the examination of a multi-temporal image series. A multi-image time-series constructed from the Landsat suite of optical sensors could (at present) theoretically consist of 35 images (1972–2006) per scene, which could be used in a continuous fashion to create "regrowth trajectories" for any forested stand disturbed since 1972. Although in some areas geographic and climatic factors may limit the availability of suitable images required to create useful trajectories of forest regrowth, it is likely the number of images needed to sufficiently capture the landscape disturbance/recovery signal will be fewer than conceptualized in this theoretical example. As forest stands in the Pacific Northwest commonly enter the stem exclusion phase (i.e., closed canopy condition) of successional development within the first 20 years after clearcutting (Franklin et al., 2002) we base our analysis of postharvest early forest successional patterns on 16 Landsat TM and 3 Landsat ETM+ images covering 18 years. This rapid rate of tree regrowth after disturbance eliminates the need to lengthen the time span of our image series back to Landsat's Multi-Spectral Scanner (MSS) system. In addition, the improved 30 m resolution of the post-MSS images better matches the resolution of our ground referenced tree cover data.

We define "trajectory" as a series of states through which a system proceeds over time. Trajectories (or change-curves) are comprised of a series of mathematical or statistical models fit to repeatedly measured observations, which are used to characterize or quantify various pathways of vegetation response to disturbance. The shape of vegetation regrowth trajectories has long been recognized by field ecologists as a practical means of describing plant community responses to various disturbance types (Armesto and Pickett, 1986; Halpern and Franklin, 1990; del Moral and Bliss, 1993), as differences in trajectory shape infer differences in the controlling mechanisms of vegetation change. Additionally, the trajectory concept forms the basis of many empirical functions commonly used by foresters to predict theoretical plant growth (Richards, 1959) and stand-level growth based on site-index (Heger, 1968).

Although the use of repeated observations collected by satellite remote sensing platforms such as Landsat seem particularly well suited to analyzing continuous trends in vegetation via trajectory analysis, only a few examples can be found in the literature (Viedma et al., 1997; Joyce and Olsson, 1999). One example is presented by Lawrence and Ripple (1999) who derive vegetation change trajectories with estimates of percent green vegetation cover predicted independently from 8 Landsat TM images (covering 15 years). These change trajectories were used to describe and quantify various regrowth pathways following the 1980 volcanic eruption of Mt. St. Helens in southwestern Washington.

Ultimately the success of the trajectory approach in capturing real vegetation change hinges on the successful radiometric calibration of the multi-temporal image series. Given this importance, we favor the use of a radiometric calibration method, which was specifically designed to operationally minimize residual scatter (i.e., lower RMSE) in early forest regrowth trajectories in western Oregon. The method, referred to as "absolute-normalization" (Schroeder et al., 2006), uses statistically selected pseudo-invariant features (see Canty et al., 2004) to relatively normalize an image time-series to an atmospherically corrected reference image (corrected with 6S, Vermote et al., 1997). All images in the multi-temporal Landsat series presented here were normalized to a common radiometric scale (across all images <0.025 RMSE), while simultaneously correcting for atmospheric and sun/sensor view-angle effects.

Once the images comprising a multi-temporal image series share a common radiometric scale, meaningful regrowth trajectories can be constructed directly from spectral reflectance values, from fraction images derived via spectral mixture analysis (Smith et al., 1990) (e.g., green vegetation, non-photosynthetic vegetation, soil and shade images) or with biophysical estimates predicted from reflectance (e.g., percent

tree cover). In this paper we base our forest regrowth trajectories on a date-invariant relationship developed between Landsat spectral data and ground measured tree cover data collected by the U.S. Forest Service Pacific Northwest (PNW) Forest Inventory and Analysis (FIA) program. Although date-invariant regression can be thought of as a form of post-classification comparison, the use of a detailed radiometric calibration procedure, continuous versus class based estimates and derivation of change information from multiple image trajectories improves on the traditional application of the method. For more details on the date-invariant regression approach, referred to as ''state model differencing'' see Healey et al. (2006).

We aim to address the following three objectives: first, we seek to corroborate the existence of divergent forest regrowth pathways among harvested stands previously identified in western Oregon via airphoto interpretation (Nesje, 1996; Yang et al., 2005). Second, we compare landscape scale early successional forest regrowth patterns between the two primary forested provinces in the study area (i.e., the moist, warm Coast Range Province and the drier and colder Western Cascade Province). Finally, we use commonly available physical proxies (e.g., aspect, slope, elevation) and plant relevant (e.g., potential relative radiation, temperature, precipitation) explanatory variables to predict early successional forest regrowth patterns in both provinces.

2. Methods

2.1. Study area

The study area is comprised of Landsat WRS-2 path 46 row 29, which covers approximately 185 km^2 of western Oregon (Fig. 1). The two main forested provinces in the study area are described by Franklin and Dyrness (1988) as the Coast Range Province (CRP) and the Western Cascade Province (WCP). The CRP is characterized in the far west by a Sitka spruce zone a few kilometers wide lying directly adjacent to the Oregon coast. The rest of the CRP and the majority of the WCP are dominated by conifers common to the Douglas-fir/western hemlock zone, although hardwood species such as red alder, vine maple, big leaf maple and Pacific dogwood can dominate moist riparian areas and dry valley margins.

In Douglas-fir forests two principal seral groups typically comprise post-disturbance vegetation communities, residuals (members of the original forest community) and invaders (non-forest species that colonize after the disturbance event) (Halpern and Franklin, 1990). Halpern (1989, Table 1) describes six forest understory communities common to Douglas-fir forests. In addition to conifer trees, early seral communities in this region can often be dominated by several grass, herb, shrub (e.g., ceanothus, oceanspray, salal, vine maple, Oregon grape, hazel and sword fern) and non-conifer tree species (bitter cherry, Pacific madrone, and chinkapin). The extent to which of these life forms dominates after disturbance is likely a function of disturbance intensity, initial seed abundance, site condition, stochastic processes (e.g., climate, seed dispersal), and forest management activities. Regardless of life form dominance, a complex mixture of several species is likely to occur until canopy closure is fully achieved.

Overall, the climate of the Pacific Northwest is typified by warm, dry summers and mild, wet winters. The study area encompasses a wide range of elevations, yielding strong physical and climatic gradients. Based on annual averages, the CRP typically receives more precipitation (3000 mm versus 2300 mm) and is warmer in the winter (5 °C versus −5 °C) and cooler in the summer (16 °C versus 23 °C) than the WCP. These

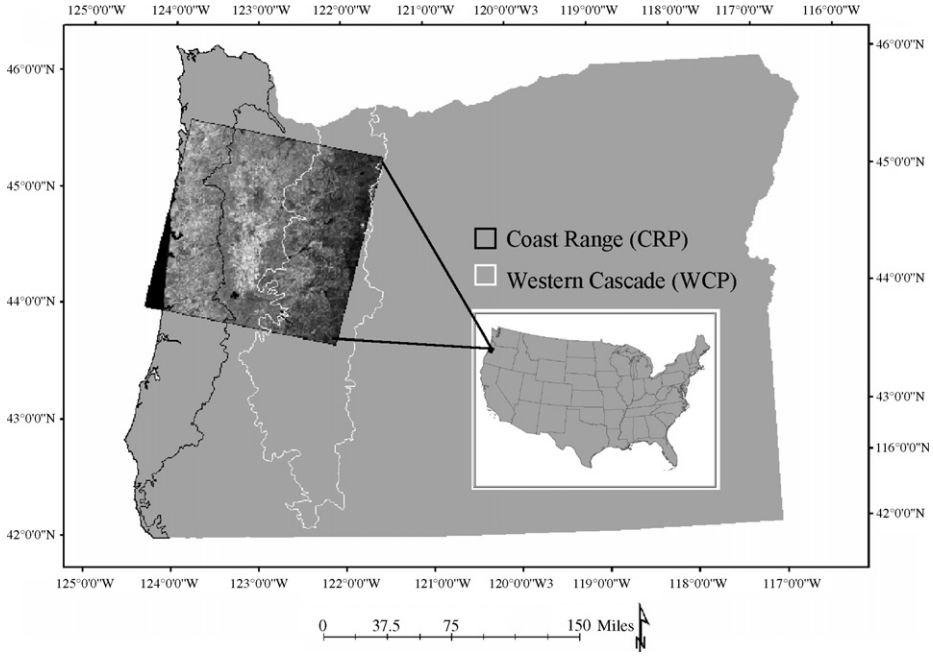

Fig. 1. Landsat WRS-2, path 46 row 29 study area showing Coast Range (CRP) and Western Cascade (WCP) ecological provinces in western Oregon, USA.

climatic differences, in concert with differences in elevation (CRP: 450–750 m versus WCP: 450–3000 m) and geologic parent materials yield a wide array of growing conditions. The study area also includes a diverse distribution of existing land ownership categories (Cohen et al., 2002), and therefore represents the disturbance and recovery patterns present in the region.

2.2. Data

2.2.1. Multi-temporal image series

Our characterization of forest regrowth patterns in western Oregon focuses on the analysis of a multi-temporal image series consisting of 19 summer (e.g., July–September), near anniversary Landsat TM and ETM+ images (WRS-2, path 46 row 29) (Table 1). A detailed description of the image selection criteria, as well as the geometric and radiometric corrections applied to the multi-temporal image series can be found in Schroeder et al. (2006). In all, the images comprising the multi-temporal image series were atmospherically corrected and normalized to within 0.025 RMSE of the selected reference image (1994) using the absolute-normalization approach detailed above. For this study the 2005 image was added to the multi-temporal image series using the same geometric and radiometric processing protocols described in Schroeder et al. (2006).

2.2.2. Tree cover

Three independently collected (one ground based, two photo-interpretation based) tree cover (measured as percent) data sets were utilized in this study. The ground measured tree cover data set was recorded by line transect method (see pages 155–162, USDA Forest Service, 1995) during the 1995 periodic forest inventory of western Oregon conducted by the U.S. Forest Service PNW-FIA program. The 2.1 ha FIA plots are coded from 1 to 5 based on the number of different land cover conditions (e.g., forest, water, non-forest) observed on each of the five measured subplots. Thus, a plot labeled 1 (referred to as single condition) would have only 1 dominant land cover condition, whereas a plot labeled 5 would have a different observed land cover condition at each measured subplot. To avoid spectral mixing with unwanted non-forest and water condition classes, we elected to use only the tree cover data collected on the single condition, forested plots ($n = 202$) falling within the Landsat 46/29 study area. Although this approach required discarding some potentially useable data, our ultimate goal was to minimize the impact of sample heterogeneity on the date-invariant tree cover regression model.

The two airphoto based tree cover data sets, which were used to validate the date-invariant tree cover regression model, were collected by two separate photo-interpreters. Both interpreters estimated percent tree cover over a fixed sample of plots repeatedly over time using an assortment of high-resolution aerial photographs (see Table 2 for photo scales and formats). Because we used a date-invariant approach to model tree cover, we elected to use photo-interpreted estimates of tree cover recorded for a given plot, at different points in time, as separate validation samples. Due to the timing of photointerpretation, quantification of interpreter to interpreter bias was not possible.

Interpreter 1 photo-interpreted percent tree cover over 125 of the same 2.1 ha single condition, forested FIA plots that make up the ground based tree cover data set. Several of these plots were re-interpreted at a second point in time, yielding 162 tree cover validation samples (Table 2). Interpreter 2 estimated percent tree cover over 153, 1 ha sample plots (see Yang et al., 2005), which including remeasurement yielded 249 tree cover validation samples (see Table 2). Overall, the two photo-interpreted tree cover data sets combined to yield a total of 411 tree cover validation samples, spanning 11 years. It is important to note that interpreter 1's photo-interpreted estimates of tree cover were taken solely from plots falling on private forest lands, whereas interpreter 2's were only from national forest lands. Thus, by combining the two data sets we not only maximized the size and temporal span of our validation sample, but also accounted for any potential differences in tree cover based on land ownership.

2.2.3. Explanatory variables

We are interested in spatially predicting patterns of forest regrowth, thus we compiled 12 geographically referenced

Table 1
Landsat WRS-2, path 46 row 29 multi-temporal image series

Sensor	Date
TM	26 August 1986
TM	12 July 1987
TM	31 August 1988
TM	3 September 1989
TM	7 July 1991
TM	10 August 1992
TM	29 August 1993
TM	31 July 1994
TM	19 August 1995
TM	21 August 1996
TM	23 July 1997
TM	11 August 1998
TM	16 August 2000
TM	25 August 2003
TM	26 July 2004
TM	29 July 2005
ETM+	22 August 1999
ETM+	26 July 2001
ETM+	29 July 2002

Table 2
Airphoto based percent tree cover validation data set

Year of photo	Interpreter	Scale	Format	*n*
1987–1988	2	1:40,000	BW	81
1989	2	1:12,000	True color	33
1990–1992	2	1:12,000	True color	18
1993–1995	2	1:12,000	True color	26
1997–1998	2	1:12,000	True color	91
1994	1	1:24,000	True color	125
2000	1	1:40,000	BW	37
Total				411

BW stands for Black and White.

explanatory variables (3 physical proxy, 9 plant relevant) for use in classification and regression tree (CART) statistical analysis. The physical proxy variables include transformed aspect (index 0–2) (Beers et al., 1966), slope (%) and elevation (meters), all derived from a 30 m DEM of the study area. Since slope, aspect and elevation are merely correlated with the moisture and temperature gradients plants commonly respond to, we refer to them as ''physical proxies''.

On the other hand, recent advances in the spatial representation of direct resource gradients such as moisture, temperature and soils allowed us to use several ''plant relevant'' variables in our analysis. These variables include, potential relative radiation (PRR) (Pierce et al., 2005), which is a unit less index at 30 m resolution used to approximate the ''potential'' incident radiation received by a given surface location during a set window of time (applied here using a 12 month growing season). Here the range of PRR is 985 (e.g., deep, north facing canyon) to 21,959 (e.g., open, slightly southern facing hill slope). The highest value (21,959) represents the location with the highest probability of receiving incident radiation in the absence of clouds. In addition to PRR, we also use PRISM temperature (parameter-elevation regressions on independent slopes model, Daly et al., 1994, http://www.prismclimate.org), July maximum and January minimum (1 km resolution) in (°C), and five CONUS (Conterminous United States) soil layers (Miller and White, 1998, http://www.soilinfo.psu.edu/index.cgi) estimated at a 1 km resolution (sand (%), silt (%), clay (%), soil depth (cm), and field capacity (kg)).

2.3. Date-invariant regression modeling

In this study we based our forest regrowth trajectories on estimates of percent tree cover derived from Landsat spectral reflectance data. This was accomplished by first developing an initial regression model between the ground measured percent tree cover data collected by PNW-FIA and the 1995 Landsat spectral reflectance data. To obtain reflectance data for each of the 202 single-condition, forested FIA plots we took the mean of a 22 pixel mask (Fig. 2) which was developed to mimic the size and shape of the FIA ground plot (for details on FIA ground plots see pages 17–38, USDA Forest Service, 1995). As FIA plot coordinates are collected on the southern portion of each plot (i.e., subplot 1), we matched each plot coordinate to the southern portion of our 22 pixel mask (gray shaded pixel in Fig. 2). Other studies, which have extracted Landsat spectral reflectance data for use with FIA data have used similar techniques (Ohmann and Gregory, 2002).

We then employed a standard correlation procedure where the extracted means of the spectral variables (Landsat bands 1–5, and 7), and subsequently derived vegetation indices [normalized difference vegetation index (NDVI) (Rouse et al., 1973), normalized difference moisture index (NDMI) (Hardisky et al., 1983; Jin and Sader, 2005) and tasseled cap (Crist and Cicone, 1984)] were evaluated via scatter plot to determine their relationship with tree cover and to explore the need for transformation. This evaluation revealed the need to linearize the Landsat bands using a common square root transformation.

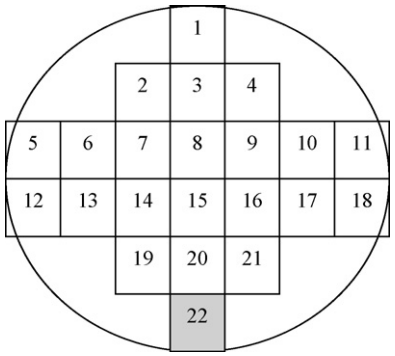

Fig. 2. Mask used to extract mean Landsat spectral data over FIA plots. Gray shading indicates the anchor pixel matched to each plot coordinate.

Stepwise multiple regression was then used to identify a preferred (i.e., high R^2, low RMSE) model. Several models were evaluated, however we determined that a three variable model containing Landsat bands 1, 3 and 7 best captured the variation in the ground measured tree cover data (see discussion). To ensure that the variance observed in our observations was adequately preserved in our predictions we preferred the use of reduced major axis regression (RMA) (Cohen et al., 2003). As in Cohen et al. (2003), we used canonical correlation analysis (CCA) to derive a linear combination of the Landsat bands identified above for use in X on Y RMA regression.

This initial RMA regression model was applied individually to the remaining 18 ''absolutely normalized'' Landsat images, which yielded a total of 19 tree cover images. This date-invariant regression approach (Healey et al., 2006) assumes that an effective radiometric calibration procedure has resulted in a common radiometric scale among all images, resulting in an date-invariant relationship between spectral reflectance and the biophysical variable of interest. To test the validity of this assumption, we conducted a leave-one out cross-validation of the initial RMA regression model ($n = 202$), as well as a temporal accuracy assessment covering 11 different tree cover images using the two airphoto based tree cover data sets (Table 2). The date-invariant tree cover estimates falling below 0% and above 100% were rescaled to fall between 0 and 100% to match the scale of the airphoto data. Mean tree cover was calculated for each of the 2.1 ha (interpreter 1) and 1 ha plots (interpreter 2) using each plots coincident tree cover image. The mean plot tree cover estimates (predicted) were then compared with the photo-interpreted tree cover estimates (observed) via linear regression. As we are primarily interested in knowing the accuracy of the percent tree cover predictions across all images (i.e., those with validation data), we opted to combine all 411 validation samples into one global validation model.

2.4. Stand disturbance maps

We are interested in using a trajectory-based approach to analyze patterns of forest regrowth following clearcut harvesting. Consequently, we mapped three sets of clearcut harvests

which we later use as spatial masks to extract pixel level tree cover estimates from our 19 tree cover images derived via date-invariant regression modeling. We decided on analyzing forest regrowth using three periods of clearcuts for two reasons. First, regrowth patterns are likely to vary from year-to-year in complex ways, so by including stands clearcut at different times we hoped to capture a broader range of regrowth variability in our analysis. Second, clearcut harvests tend to occur on relatively small (e.g., <10 ha), scattered blocks over the landscape, so by developing regrowth trajectories over clearcuts occurring in different years we effectively increase the number of stands, as well as the spatial area available for statistical analysis.

The three sets of clearcuts occurring between 1986–1987, 1987–1988 and 1988–1989 (hereafter referred to as periods 1–3) were mapped independently using RGB color composite analyses (Coppin et al., 2004) of Landsat band 5 and a minimum distance to means supervised classifier (Lillesand et al. (2004)). As in Cohen et al. (1998), each stand disturbance map was first smoothed using a 7×7 majority filter to rid of unwanted noise (i.e., single pixels classified as clearcuts). We then used the ERDAS Imagine clump function to identify and group contiguous groups of clearcut pixels, and finally used the ERDAS Imagine sieve function to eliminate all clearcuts less than 2 ha in size. The three stand disturbance maps were then hand-edited using several of the high resolution aerial photographs from Table 2 as reference. Areas classified as forest change but were determined not to be clearcuts were removed to ensure a high level of overall quality. Although we did not explicitly evaluate the accuracy of the stand disturbance maps, similar methods for mapping clearcut harvests occurring in Oregon west of the Cascade crest have achieved upwards of 90% accuracy (Cohen et al., 2002).

2.5. Forest regrowth class trajectories

To spatially derive forest regrowth trajectories for the clearcuts identified from the supervised classification we first stacked the geographically referenced tree cover images derived via date-invariant regression modeling into three multi-temporal image stacks, one for each period of mapped clearcuts. The first tree cover image in each multi-temporal stack corresponds to the first growing season after each period's mapped harvest disturbances. For period 1, the multi-temporal stack contained a total of 17 tree cover images, the first tree cover image corresponding to 1988. For subsequent periods the multi-temporal tree cover stacks contained 16 and 15 tree cover images respectively. The stand disturbance maps were then used to mask (i.e., isolate) the pixel level tree cover values from each period's respective tree cover stack.

The extracted time-series of pixel level tree cover estimates were then grouped into 20 individual "regrowth" classes using the ISODATA clustering algorithm in ERDAS Imagine. To facilitate clustering, each period's multi-temporal tree cover stack was clustered separately as each had a different number of tree cover images. Using the statistical measure of transformed divergence (Jensen, 1996) the spectral separability of the 20 "regrowth" classes was evaluated. In general, separability analysis is used in image classification to determine the extent to which clustered class-mean values overlap each other in spectral space. Here separability analysis revealed the need to combine several of the "regrowth" classes as they were not spectrally unique. This process resulted in the creation of five statistically discrete forest regrowth classes per period. The four main classes were visually assigned labels based on observed rates of percent tree cover increase, which included little to no regrowth, slow regrowth, moderate regrowth, and fast regrowth. The fifth class, labeled mixed regrowth, was interpreted to contain a highly variable mixture of partially harvested areas, prescribed burns and shadows. These areas commonly have a dark spectral appearance, resulting in a false signal of high initial tree cover immediately following clearcutting. Thus, given its highly variable nature, as well as its limited spatial extent, we exclude the mixed regrowth class from the remainder of the analysis.

2.6. Forest regrowth spatial pattern analysis

To corroborate the presence of divergent pathways of forest regrowth in western Oregon we summarized the pixel level frequency distribution of the four main forest regrowth classes identified from ISODATA clustering according to area disturbed by clearcut harvest and by topographic position. These distributions were used as a means of describing the landscape scale, forest regrowth signal for both the CRP and WCP. To make meaningful comparisons of forest regrowth between the two ecological provinces we attempted to normalize the differences in harvest area between the CRP and WCP by basing our frequency distributions on the "percent of clearcut area" metric, which we calculated using the following equation:

$$\%\,\text{of clearcut area} = \frac{\text{TAFRC}}{\text{TACHP}} \times 100 \quad (1)$$

where TAFRC is the total area of each forest regrowth class, TACHP is the total area clearcut per harvest period. With three periods of clearcuts available for analysis, we were able to use this metric to characterize the landscape scale forest regrowth patterns occurring in each ecological province. To gain further inference into the patterns of forest regrowth associated with the geographically referenced environmental attributes we also summarized the patterns of forest regrowth in the CRP and WCP according to three relevant topographic variables (i.e., aspect, slope, elevation). For ease of display, the topographic variables were binned into class groupings (e.g., aspect 1–33° labeled as N–NE class). For each topographic class grouping, the distribution of each forest regrowth class was based on "percent of clearcut area" as above, except the mean value observed over all three periods is reported (error bars are across period standard deviations).

2.7. Classification and regression tree modeling

To formulate a better understanding of the environmental attributes influencing forest regrowth following clearcut harvesting in western Oregon we attempted to predict forest

regrowth rates for both the CRP and WCP using the aforementioned explanatory variables and CART statistical modeling. We select CART as it is flexible, non-parametric, and robust to complex non-linear relationships (Friedl and Brodley, 1997) and has been previously used to examine changes in vegetation (Lawrence and Ripple, 2000; Lutz and Halpern, 2006). Since CART modeling is typically data intensive, we decided to combine the three periods of regrowth classes into one spatial layer to maximize the available land area from which to draw our statistical sample. In an attempt to keep training data equal among regrowth classes (Lawrence and Wright, 2001) we used a stratified random design (separately for the CRP and WCP) to select approximately 300 pixels per regrowth class (4 classes) to be used as training samples. An additional ≈300 samples per regrowth class were selected (separately for the CRP and WCP) for the purpose of testing the predictive power of the developed CART models. Overall, a total of 2375 (1186 testing, 1189 training) samples were derived for the CRP and 2371 (1183 testing, 1188) for the WCP. For each sample location, the explanatory variables were extracted on a per pixel basis for use in statistical modeling.

Using the tree modeling tools in S-plus we developed CART models for both the CRP and WCP. In S-plus, terminal nodes are created either when the total number of observations at the node is less than 10 or the deviance at the node is less than 1% of the total deviance for the entire tree (Venables and Ripley, 1997). Since CART models tend to over-fit the data, it is crucial that they be pruned back to some degree to avoid over-fitting, but not to a point that affects the robustness of the model. To determine an appropriate size for our tree models we elected to use a cross validation procedure (Venables and Ripley, 1997; Lawrence and Wright, 2001) where each set of training samples is divided into 10 equal parts. Trees are fit iteratively for 9 of the 10 trees, with the tenth being used as validation. After all the trees have been fit, the minimum average deviance suggests a suitable number of nodes for the final tree. Although an analyst may opt to use a smaller size tree than suggested by cross validation, we found the suggested tree sizes to be acceptable for both the CRP and WCP models. The final tree models contained 10 (CRP) and 6 (WCP) terminal nodes and were plotted so that branch size was roughly proportional to the deviance explained by each node.

To assess the accuracy of both CART models we used the test samples to compute standard confusion matrices with overall, producers, and users accuracies, as well as Kappa (Congalton, 1991), and Tau (Ma and Redmond, 1995) statistics. In addition, the accuracy of both CART models was evaluated using an aggregated approach, where the four regrowth classes were combined to represent "fast" (i.e., combine fast and moderate regrowth classes) and "slow" (i.e., combine little to no and slow regrowth classes) forest regrowth conditions.

3. Results

3.1. Initial tree cover model

Model parameters for the initial tree cover regression model developed using the 202 single condition, forested FIA ground measured field plots and the linear combination of spectral variables (bands 1, 3 and 7) from the 1995 Landsat TM image are found in Table 3. Using a leave one out cross-validation procedure (Cohen et al., 2003) we found the RMA regression model to be highly significant both in terms of variance explained ($R^2 = 0.77$) and predicted error (RMSE = 14.15). The predicted (from cross-validation) versus observed tree cover is presented in Fig. 3. The selection of RMA regression ensured that nearly all the original variation found in our observations was preserved in our tree cover predictions (variance ratio = 1.00). The near zero bias (0.03) indicated that overall there is no over- or under-prediction of tree cover in our initial model.

Table 3
Regression parameters for the initial percent tree cover and airphoto validation models

Model	n	Slope	Intercept	Mean	Bias	R^2	RMSE
Initial RMA	202	1.14	−9.66	70.97	0.03	0.77	14.15
Airphoto validation	411	0.94	3.66	69.38	0.00	0.68	16.09

3.2. Date-invariant regression

The temporal accuracy of our date-invariant regression approach was assessed using the two airphoto based tree cover data sets which contained coincident measurements with 11 of the 19 tree cover images (Table 2). Using 411 airphoto based validation samples we incorporated data from all 11 tree cover images into one global validation model (Table 3 for regression model parameters). The scatter plot of predicted (from date-invariant regression) versus observed (airphoto interpreted) tree cover is presented in Fig. 4. Overall, we found good agreement between the airphoto interpreted measures of percent tree cover and those derived via our date-invariant regression modeling approach. Both the amount of explained variance ($R^2 = 0.68$) as well as the predicted error (RMSE = 16.09) were found to be similar to those observed in the initial tree cover model. The selection of RMA regression ensured that nearly all the variation found in our validation plots was preserved in our tree

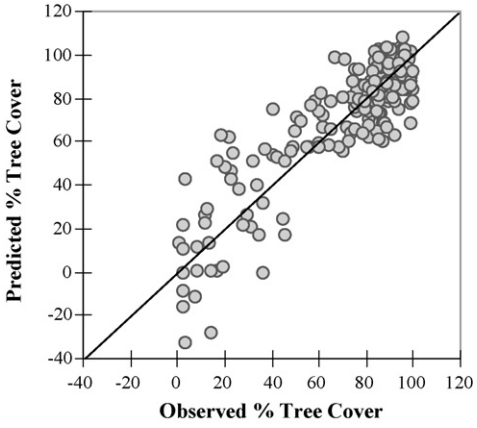

Fig. 3. Predicted (from cross-validation) vs. observed percent tree cover from initial RMA regression model ($n = 202$). Solid line is 1:1.

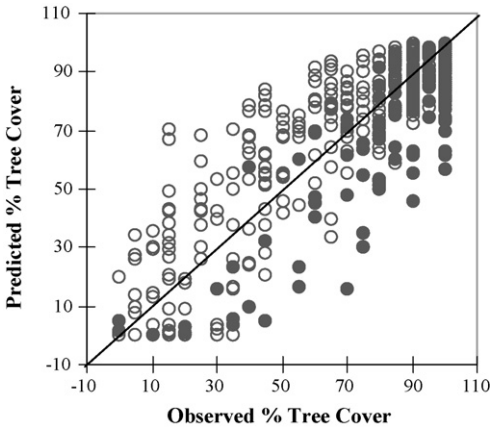

Fig. 4. Predicted (from date-invariant regression) vs. observed percent tree cover from airphoto interpretation data. Filled circles represent interpreter 1 ($n = 162$), open circles interpreter 2 ($n = 249$). Solid line is 1:1.

cover predictions (variance ratio = 1.00). Furthermore, the near zero bias observed in the global validation model indicates that there is no bias in the relationship between date-invariant regression and airphoto based tree cover.

3.3. Forest regrowth class trajectories

Each period's mapped clearcuts were spatially clustered into statistically meaningful forest regrowth classes (i.e., little to no, slow, moderate, fast) using ISODATA clustering. The mean values of each period's forest regrowth classes were fit with third-order polynomial curves, resulting in three fitted curves per forest regrowth class (Fig. 5). These curves, or "mean forest regrowth trajectories" were visually compared for each regrowth class and were found nearly indistinguishable across harvest periods. As a result, we determined that each period's forest regrowth classes could be used interchangeably in the CART analysis.

3.4. Forest regrowth patterns

For the CRP and WCP we used "percent of clearcut area" to summarize forest regrowth at the landscape scale for each clearcut harvest period (Fig. 6). The consistent patterns of forest regrowth observed over the three clearcut periods indicate a much higher percentage of fast regrowth in the CRP as opposed to a much higher percentage of little to no regrowth in the WCP.

Frequency distributions of forest regrowth were also derived for three topographic variables of interest (aspect, slope, and elevation). Forest regrowth by aspect class is presented in Fig. 7. For both the CRP and WCP the highest percentage of fast regrowth occurred on north facing aspects (i.e., N–NE, NE, NW, and N–NW), with nearly twice as much fast regrowth being observed on the northern aspects of the CRP then on the WCP. On the other hand, both ecological provinces saw the percentage of little to no and slow forest regrowth classes increase on southern facing aspects (SE, S–SE, S–SW, SW). Although this general trend was observed for south facing aspects in both ecological provinces, the WCP was found to have more than triple the amount of little to no and slow regrowth on southern aspects than the CRP.

Forest regrowth by percent slope class is presented in Fig. 8. For both ecological provinces, as slope class increased past 10–

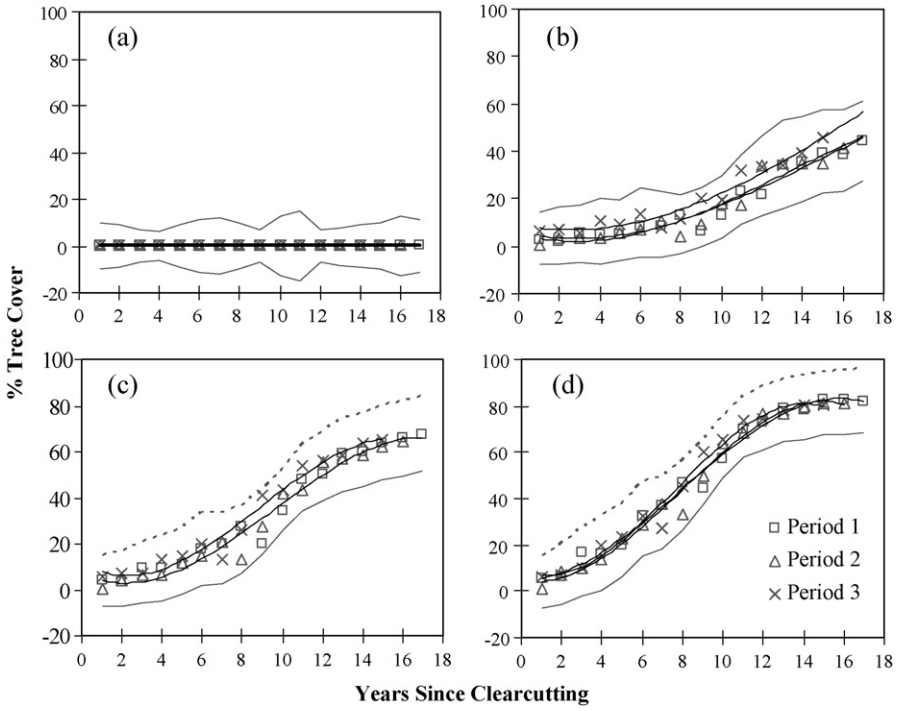

Fig. 5. Mean forest regrowth trajectories for (a) little to no, (b) slow, (c) moderate, and (d) fast regrowth classes. Solid lines are fitted third order polynomial curves; dashed lines are the average across period standard deviations.

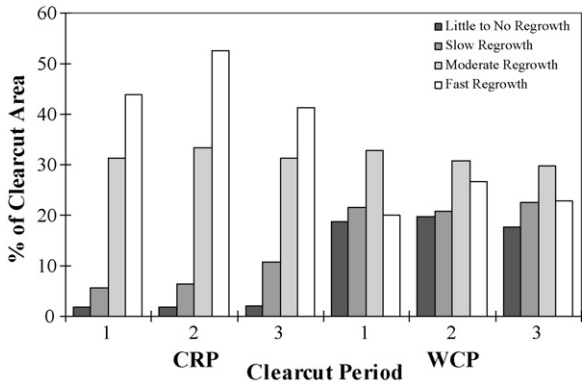

Fig. 6. Landscape scale forest regrowth patterns based on the percentage of clearcut area (i.e., (area of each forest regrowth class/total area clearcut per harvest period)×100). Clearcuts were mapped between 1986 and 1987 (period 1), 1987 and 1988 (period 2), and 1988 and 1989 (period 3).

19% the amount of fast regrowth tended to decrease. For the WCP, this observed decrease in fast regrowth was more pronounced than for the CRP and was also accompanied by a noticeable increase in the amount of little to no and slow forest regrowth. Other than the observed decrease in fast regrowth with increasing slope, the remaining forest regrowth distributions in the CRP were found to be relatively stable across slope classes.

Forest regrowth by elevation class is presented in Fig. 9. For both ecological provinces, the percentage of fast regrowth noticeably decreased as elevation increased. This pattern seemed more pronounced for the WCP as clearcut harvesting occurred over a much higher elevation range. Although fast regrowth decreased with elevation in the CRP, at no time did the percentage of little to no regrowth exceed fast regrowth. On the other hand, little to no regrowth significantly exceeded fast regrowth in the WCP at all elevations above 762 m.

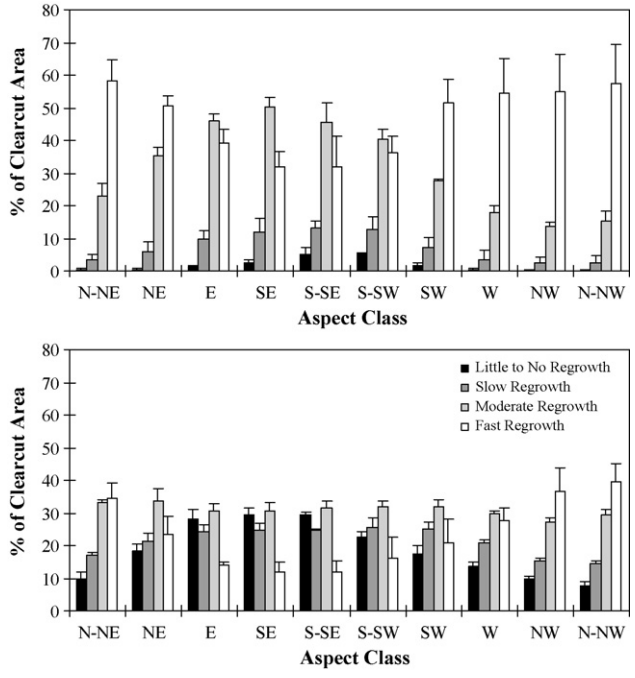

Fig. 7. Patterns of forest regrowth according to aspect class. Top panel is CRP, bottom panel is WCP. Error bars represent across period standard deviations.

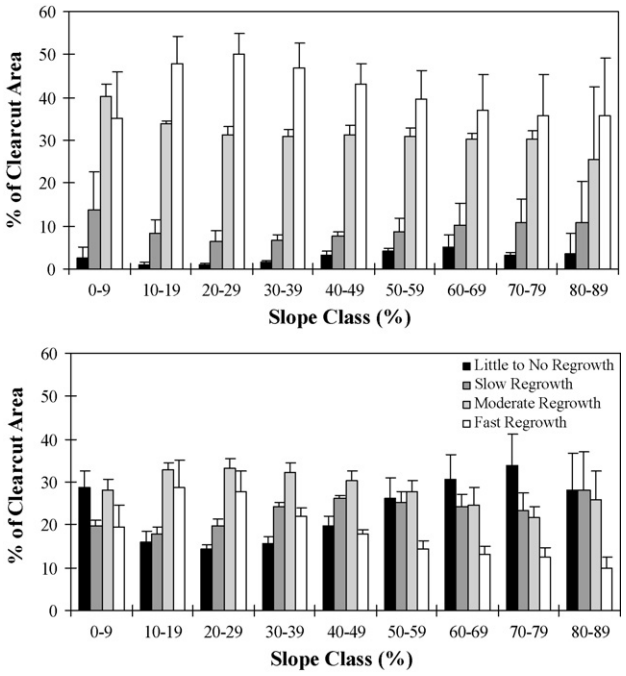

Fig. 8. Patterns of forest regrowth according to slope class. Top panel is CRP, bottom panel is WCP. Error bars represent across period standard deviations.

3.5. CART models

Using the 12 explanatory variables we constructed CART classification models to predict the forest regrowth classes of

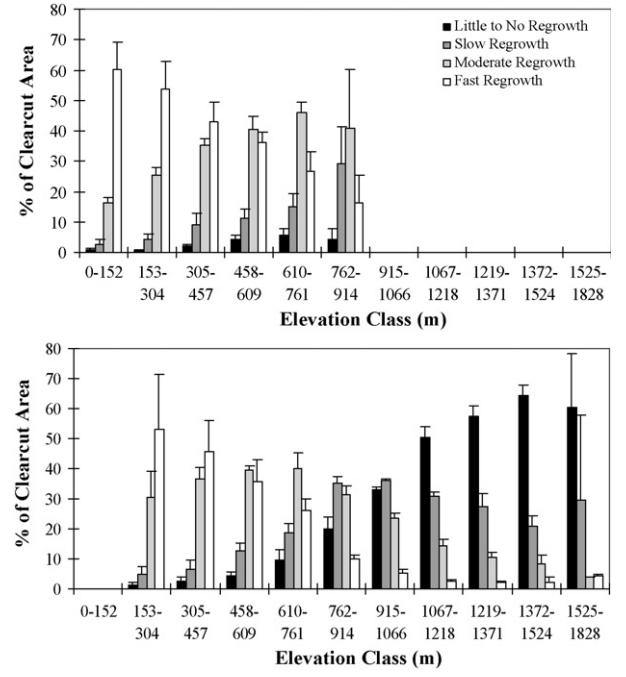

Fig. 9. Patterns of forest regrowth according to elevation class. Top panel is CRP, bottom panel is WCP. Error bars represent across period standard deviations.

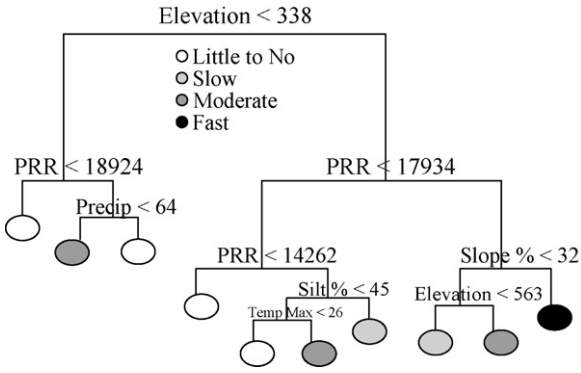

Fig. 10. CART classification tree model for the CRP. Elevation is in m, precipitation in mm and temperature in °C. See section on explanatory variables for description of PRR.

the CRP and WCP ecological provinces. Six of the explanatory variables (elevation, PRR, percent slope, PRISM average annual precipitation, CONUS soil silt, and PRISM July average maximum temperature) were used to construct the final CRP CART model (Fig. 10), which yielded 10 terminal nodes or classification decision rules. Branch length of the tree indicated that elevation explained the largest percentage of variation in CRP forest regrowth classes, followed by PRR and percent slope. In the CRP, fast forest regrowth was generally predicted to occur on low elevation sites (<338 m) and on high elevation sites (>338 m) with relatively low radiation exposure (PRR <14,262). Little to no forest regrowth was predicted only on high elevation (>338 m) sites having both high radiation exposure (PRR >17,934) and steep topography (slope (%) >32). A variety of other combinations of the six explanatory variables resulted in predictions of the moderate and slow forest regrowth classes.

The overall accuracy of the CRP CART model was 46% (Table 4). According to Landis and Koch (1977) a κ of 27% suggests ''fair agreement'' between the predicted regrowth classes and test samples. The Tau statistic indicates that 27% more pixels were classified correctly than would be expected by random assignment. Ranging from 17 to 79%, the individual class accuracies (Table 4) suggested that the maximum and minimum regrowth classes (i.e., little to no and fast) were predicted with greater accuracy than the classes falling in between (i.e., slow and moderate).

Table 4
Classification error matrices for the CRP and WCP CART models

	Little to no	Slow	Moderate	Fast	Producers (%)	Users (%)
CRP						
Little to no	**150**	40	57	34	58	53
Slow	70	**50**	101	82	37	17
Moderate	30	30	**100**	138	34	34
Fast	10	15	40	**242**	49	79
WCP						
Little to No	**189**	57	29	3	49	68
Slow	136	**93**	60	15	38	31
Moderate	51	66	**88**	101	35	29
Fast	8	31	71	**190**	61	63

	CRP (%)	WCP (%)
Overall	45.58	47.14
κ	27.00	29.00
τ	27.44	29.51

Bold values indicate correct classification.

Four of the explanatory variables (elevation, PRR, PRISM July maximum temperature, and PRISM January minimum temperature) were used to construct the final WCP CART model (Fig. 11), which yielded six terminal nodes or classification decision rules. Branch length of the tree indicated that elevation and PRR explained the largest percentage of variation in the WCP forest regrowth classes. In the WCP, fast forest regrowth was generally predicted to occur on low elevation (<805 m) sites having moderate to high radiation exposure (PRR <18,924) and warm winter minimum temperatures (January minimum temperature >0 °C). Little to no forest regrowth was predicted to occur on high elevation sites (>1014 m) and on moderately high elevation sites (>805 and <1014 m) with low summer maximum temperatures (July maximum temperature <24 °C). A variety of other combinations of the six explanatory variables resulted in predictions of the moderate and slow forest regrowth classes.

The overall accuracy of the WCP CART model was 47% (Table 4). A κ of 29% suggests ''fair agreement'' between the predicted regrowth classes and the test samples (Landis and Koch, 1977). The Tau statistic indicates that 30% more pixels were classified correctly than would be expected by random assignment. Ranging from 29 to 68%, the individual class accuracies (Table 4) suggested that the maximum and minimum regrowth classes (i.e., little to no and fast) were predicted with greater accuracy than the classes falling in between (i.e., slow and moderate).

Since the maximum and minimum regrowth classes (i.e., little to no and fast) showed greater predictive potential, we reassessed the accuracy of the CART models using an ''aggregated'' approach. This was accomplished by combing the fast and moderate regrowth classes to represent ''fast'' forest regrowth and the little to no and slow regrowth classes to represent ''slow'' forest regrowth. Using the aggregated

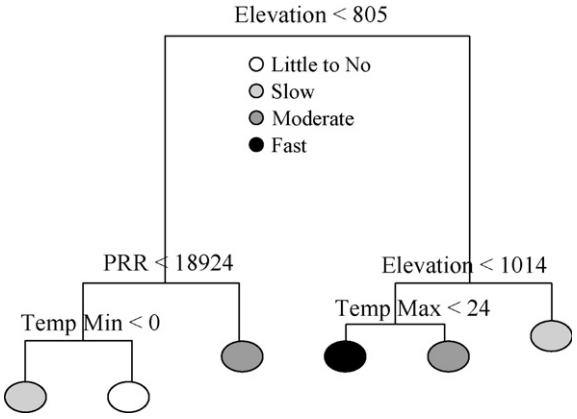

Fig. 11. CART classification tree model for the WCP. Elevation is in m and temperature in °C. See section on explanatory variables for description of PRR.

Table 5
Aggregated classification error matrices for the CRP and WCP CART models

	Slow	Fast	Producers (%)	Users (%)
CRP				
Slow	**310**	274	78	53
Fast	85	**520**	65	86
WCP				
Slow	**475**	107	75	82
Fast	156	**450**	81	74

	CRP (%)	WCP (%)
Overall	69.81	77.86
κ	39.25	55.78
τ	39.60	55.72

Bold values indicate correct classification.

approach the CRP model yielded an overall accuracy of 70% (Table 5). Landis and Koch (1977) suggest that a κ of 39% represents ''fair agreement'' between the predicted regrowth classes and the test samples. The Tau statistic indicates that 40% more pixels were classified correctly than would be expected by random assignment. The WCP model improved to an overall accuracy of 78% (Table 5). A κ of 56% is interpreted by Landis and Koch (1977) as a ''moderate agreement'' between the predicted regrowth classes and the test samples. The Tau statistic indicates that 56% more pixels were classified correctly than would be expected by random assignment. As expected, both the CRP and WCP overall accuracies improved with the implementation of the aggregated approach. The Tau statistics indicate that when the CART decision rules are used to predict the aggregated ''fast'' and ''slow'' forest regrowth classes the resulting classifications yield 12% (CRP) and 26% (WCP) more correctly classified pixels than classification of the four regrowth classes.

4. Discussion

4.1. Date-invariant regression

Using date-invariant regression to create meaningful forest regrowth trajectories relies heavily on a thorough radiometric calibration of the multi-temporal image series and the creation of a significant initial regression model of the biophysical variable of interest. Although a larger sample of airphoto based tree cover data was available, we opted to develop our initial regression model (Table 3, Fig. 3) with the field measured tree cover data collected by the U.S. Forest Service PNW-FIA program. This decision was based on the fact that photo-interpreted percent tree cover often contains significant interpreter bias, which if extrapolated forward via date-invariant regression could jeopardize the creation of meaningful forest regrowth trajectories. This bias is readily apparent in our airphoto validation of the initial tree cover model shown in Fig. 3, where interpreter 1 (filled circles) had a tendency to under predict and interpreter 2 (open circles) over predict percent tree cover, especially in the 20–80% tree cover range. Had both interpreters shared the same directional bias the validation of our initial tree cover model might have been less satisfying. As it stands, our validation model serves as an illustration of why field measured biophysical variables are critically important to the accurate modeling of vegetation with remotely sensed imagery. In addition, use of spectral bands 1 (visible blue, responds to forest type and serves as a measure of overall ''brightness''), 3 (visible red, responds to chlorophyll absorption in vegetation) and 7 (short-wave infrared, responds to vegetation shadowing and moisture) in our initial tree cover model demonstrates the utility of multi-wavelength sensors like Landsat at resolving useful spectral information directly pertaining to forested systems (Cohen and Goward, 2004).

Given the wide variation of life forms likely present after clearcutting it is likely that some of the error in our initial tree cover model resulted from the use of total tree cover. Utilizing separate hardwood and softwood tree cover categories could possibly improve both the fit of the initial tree cover regression model, as well as the detail with which the compositional changes associated with postharvest forest succession could be successfully resolved with an image time-series. Other potential improvements include the use of image transformation methods such as spectral mixture analysis (Smith et al., 1990), which separates and quantifies sub-pixel scene components such as green foliage, tree bark, and shadow to estimate fractional vegetation cover. Trajectories constructed of fractional images from SMA may help to more fully resolve the complex mixtures of species (deciduous versus conifer) and vegetation cover (low versus high) typically found in early successional forests of the Pacific Northwest (Sabol et al., 2002).

Although analysis with multi-temporal image series can be time consuming, one major advantage to their use is that variations from atmospheric effects and vegetation phenology, which can seriously impact change estimates based on year-to-year image differences are minimized as the overall estimate of change is based on the fitted trajectory curve (or curve class in this case). In this sense, year-to-year variations are viewed as residuals around each classes fitted trajectory. While residuals resulting from atmospheric effects and vegetation phenology are viewed as ''error'' in terms of the trajectory model, the overall pattern of regrowth is not assumed to be effected unless the curve fit is unusually low. The lowest R^2 of all four of our forest regrowth class trajectories was .93, indicating minimal year-to-year impacts from residual error at the class level. At the pixel level, we found a high level of agreement ($R^2 = .96$, RMSE = 6.05) between average pixel tree cover estimates (selected randomly across all images) and tree cover predicted from the forest regrowth curves ($n = 240$). The standard deviations of the average pixel tree cover estimates fell within the average across period standard deviations of our forest regrowth trajectories (Fig. 5), indicating that phenology effects did not prevent the forest regrowth curves from capturing the response of the original pixel values.

In general, our date-invariant regression approach improves on similar change detection techniques such as post-classification comparison (Coppin et al., 2004), which rely on simple image differencing of two or more independently produced

classifications to estimate forest change. Here we derive a more meaningful characterization of continuous forest change after clearcut harvest by employing a robust radiometric calibration procedure specifically designed to reduce the residual scatter in forest regrowth spectral trajectories (Schroeder et al., 2006) and by basing our estimates of forest change on continuous trajectories of percent tree cover. Although here we binned the continuous tree cover trajectories into forest regrowth change classes, the trajectory approach also lends itself to more detailed quantification of forest regrowth information through parameterization of the fitted mean trajectory curves (Fig. 5) (Lawrence and Ripple, 1999; Yang et al., 2005).

4.2. Patterns of forest regrowth after clearcut harvesting

It was presumed that forest succession was initiated in our study by stand-replacing disturbance from clearcut harvesting, after which vegetation communities are thought to shift from ephemeral herbaceous life forms to taller perennial shrubs and finally trees (Franklin et al., 2002). These stages of successional development which are common to western Oregon have been previously classified with percent tree cover trajectories from repeated airphoto interpretation (Yang et al., 2005), where shrub and herb dominance lasts until roughly 30% tree cover is achieved, at which time semi-closed conditions persist until canopy closure ($\geq$70% tree cover). Upon inspection, the endpoints of our forest regrowth class trajectories (Fig. 5) derived by date-invariant regression seem to coincide well with these previously defined successional stage classes (e.g., little to no forest regrowth class corresponds to open and shrub/herb successional stages; slow forest regrowth class corresponds to the end of shrub/herb successional stage; moderate forest regrowth corresponds to semi-closed forest successional stage; and fast forest regrowth class corresponds to closed canopy forest successional stage). The similarity with which patterns of continuous forest succession can be classified with airphoto and satellite based tree cover trajectories suggests that our date-invariant regression approach has successfully extended the forest regrowth trajectory concept to the spectral space of Landsat.

In terms of forest succession, our forest regrowth classes derived by date-invariant regression indicated that a wide range of successional stages could be found in both the CRP and WCP 18 years after clearcut harvesting. The large difference in tree cover regrowth rates between the little to no (Fig. 5a) and fast forest regrowth (Fig. 5d) classes substantiates previous findings that rates of vegetation recovery after disturbance in western Oregon can be highly variable (Halpern, 1988; Myster and Pickett, 1994; Nesje, 1996; Lutz and Halpern, 2006). Because our forest regrowth classes were explicitly defined in Landsat spectral space, we were able to summarize the landscape patterns of forest regrowth after clearcut harvesting at the pixel scale using frequency distributions (Figs. 6–9) based on the ''percent of clearcut area'' metric (i.e., (area of each forest regrowth class/total area clearcut per harvest period)$\times$100).

Examination of the forest regrowth class distributions in Fig. 6 indicate that 18 years after clearcut harvest a much higher proportion of disturbed forest land returned to semi-closed and closed canopy conditions in the CRP ($\approx$70%) than in the WCP ($\approx$50%). Conversely, a much higher proportion of disturbed land persisted in open or semi-closed condition in the WCP ($\approx$34%) than in the CRP ($\approx$10%). Similar distributional patterns of forest regrowth have been previously observed for the CRP and WCP (Yang et al., 2005), and are further substantiated here based on the high degree of distributional consistency observed across three periods of forest clearcuts (Fig. 6).

As our forest regrowth trajectories were derived in Landsat spectral space, we could further examine the landscape distribution of forest regrowth in relation to several topographic variables thought to influence vegetation growth rates. These distributions revealed several ecologically interpretable patterns in forest regrowth after clearcut harvesting, such as a decrease in fast and increase in slow forest regrowth on southerly aspects (Fig. 7), on steeper slopes (Fig. 8) and at higher elevations (Fig. 9). In general, the rate of forest regrowth seemed most effected by elevation (i.e., as elevation increased rate of forest regrowth tended to get slower) and least affected by steepness of slope (i.e., forest regrowth classes were distributed somewhat evenly across slope classes). It is possible that spectral variation associated with sun-angle effects could be contributing to the detection of slower regrowth on southern aspects (e.g., more sun on southern exposures will brighten the spectral signal, resulting in the prediction of less tree cover). Using only the FIA plot data ($n = 54$) we found no statistical difference at the 95% confidence level (ANOVA, $F = 1.15$, $p = 0.30$) between mean tree cover of young stands (<20 years of age) located on northern and southern aspects. Given the small sample size, we draw the conclusion that more work is needed to fully understand the effect of sun-angle on the characterization of forest regrowth rates with optical satellite imagery.

Overall, both the forest regrowth class trajectories (Fig. 5) and the frequency distributions of the forest regrowth classes (Figs. 6–9) indicated that forest regrowth rates after clearcut harvesting in western Oregon varied both within and across ecological provinces. At the landscape scale we attributed some of the across province variability in forest regrowth rates to climatic and vegetative differences between the CRP and WCP. With a longer and more favorable growing season (i.e., more annual rainfall and deep, rich soils) the CRP was found to have a larger proportion of fast forest regrowth than observed in the WCP, which is much drier and warmer during the summer growing season (Franklin and Dyrness, 1988). We also observed elevation as a potential limiting factor to forest regrowth (Fig. 9), which could explain in part the propensity for little to no and slow forest regrowth in the more mountainous WCP. Within-province differences in forest regrowth after clearcut harvest are likely the result of local site conditions, as well as forest management practices.

4.3. Predicting rates of postharvest forest regrowth with CART

The extension of forest regrowth trajectories to the spectral space of Landsat provided the opportunity to more fully

investigate the climatic and topographic attributes influencing the rate of forest regrowth following clearcut harvesting in western Oregon. Although the overall accuracies of the CART models were not high in terms of correctly classified test samples (Tables 4 and 5), the resulting classification decision rules provided interesting insights into the geographically referenced environmental attributes influencing forest succession in both ecological provinces. The CRP CART model (Fig. 10) had more decision pathways or terminal nodes (10) than the WCP CART model (6) (Fig. 11), indicating that more favorable growing conditions common to the CRP could possibly result in more complex interactions among plant relevant and physical proxy variables influencing postharvest forest regrowth. Another possibility is that more subtle environmental gradients influencing forest regrowth may not be detectable with simple dichotomous models like CART. As both physical proxy (aspect, slope and elevation) and plant relevant (precipitation, temperature, soil silt, radiation) explanatory variables were input into the CART models, the relative importance of each type of predictor could be implied based on model inclusion, whereas the relative importance of each selected predictor could be assessed according to the amount of variance explained (i.e., branch length in Figs. 10 and 11).

The importance of plant relevant predictor variables is apparent as five of the seven predictor variables selected for use in both CART models are known to directly influence forest growth (PRR radiation, PRISM average annual precipitation, PRISM July maximum temperature, PRISM January minimum temperature, and CONUS soil silt). Of the explanatory variables selected, three (elevation, PRR, PRISM July maximum temperature) were used in both the CRP and WCP models. Elevation was found to explain the largest percentage of variation in both forest regrowth models. Although elevation is not known to directly influence forest regrowth, it has been shown to influence air and soil temperatures, length of growing season, amount of damage from wind and snow, and amount of moisture from orographic precipitation (Nesje, 1996). PRR explained the next largest amount of variation in both CART models, indicating that radiation variables such as PRR which integrate annual changes in solar orientation and shading effects from local topography are likely more effective at capturing landscape radiation patterns than commonly used physical proxies (i.e., slope and aspect) (Lookingbill and Urban, 2005; Pierce et al., 2005). Interestingly the interaction between elevation and radiation has been previously found to be a limiting factor to postharvest forest successional rates in western Oregon (Cleary et al., 1978). Summer temperature was also used by both CART models, indicating that even at relatively coarse spatial resolutions (1 km) useful climatic patterns can still be resolved.

Since both CART models yielded only ‘‘fair agreement’’ (as measured by Kappa; Landis and Koch, 1977) between the predicted forest regrowth classes and the test samples we combined the four forest regrowth classes into two general ‘‘fast’’ and ‘‘slow’’ categories to gauge the statistical effectiveness of predicting more generalized postharvest forest regrowth rates. Based on the Tau statistic, the CART models correctly classified a higher percentage of test samples than classification of the four forest regrowth classes, suggesting that more general regrowth classes may be more predictable at the landscape scale.

5. Conclusion

The rate at which forest vegetation re-establishes dominance after clearcut harvesting can impact many ecological processes. Although knowing a forest stand’s current state of succession is useful, a more robust characterization can be achieved with the use of continuous trajectories developed with time-series data. A useful methodology was presented which uses a Landsat image time-series to more fully understand the spatial extent, as well as the environmental attributes influencing postharvest forest regrowth rates in western Oregon forests.

Our methodology required that the Landsat image time-series be transformed to a more meaningful biophysical measure (i.e., percent tree cover). This was accomplished through date-invariant regression, which is the extrapolation of an initial regression model developed between a single Landsat image and ground measured data to a series of cross-normalized images. Here we extrapolated an initial percent tree cover model to 19 images, which had been previously calibrated to a common radiometric scale using the ‘‘absolute-normalization’’ approach of Schroeder et al. (2006). The accuracy of the resulting tree cover estimates were successfully evaluated across time using two sets of photointerpreted tree cover data. Three periods of clearcut harvests were mapped and used to extract tree cover estimates, which were subsequently classified into four main rate classes (little to no, slow, moderate and fast). These forest regrowth rate classes were then used to develop frequency distributions describing the landscape patterns of forest regrowth in western Oregon.

The patterns of forest regrowth observed over the three clearcut periods indicated a much higher percentage of fast regrowth in the CRP and a much higher percentage of little to no regrowth in the WCP. For both ecological provinces we observed the propensity for faster regrowth on north facing aspects, shallow slopes and at low elevations. Overall, the forest regrowth classes and the frequency distributions indicated that a wide range of successional stages could be found in both the CRP and WCP 18 years after clearcut harvesting. This wide range in successional stage classes corroborates previous findings that rates of forest regrowth after disturbance in western Oregon can be highly variable (Halpern, 1988; Myster and Pickett, 1994; Nesje, 1996; Lutz and Halpern, 2006). The development of forest regrowth trajectories using spectral data from Landsat provided an opportunity to use CART statistical analysis to more fully investigate the climatic and topographic attributes influencing postharvest forest regrowth rates in western Oregon.

Both CART models provided ecologically interpretable insights into the environmental attributes influencing forest regrowth rates in both ecological provinces. Elevation followed by relative radiation expressed by PRR explained the largest amount of variation in forest regrowth, substantiating previous

findings that elevation and radiation interact to influence local site factors limiting postharvest successional rates (Cleary et al., 1978). We observed only ''fair agreement'' (as measured by Kappa; Landis and Koch, 1977) between predicted forest regrowth classes and the test samples, however when combined into two general ''fast'' and ''slow'' categories the CART models correctly classified 12% (CRP) and 26% (WCP) percent more test samples than classification of the four regrowth classes. Overall, the CART models yielded ecologically interpretable results regarding the environmental attributes (both physical proxy and plant relevant) influencing landscape scale early forest successional patterns in western Oregon.

Acknowledgments

We gratefully acknowledge data and financial support provided by the USDA Forest Service Pacific Northwest Research Station's Forest Inventory and Analysis Program. The authors also wish to thank Pacific Northwest Research Station's Scott Powell for assistance with the CART statistical modeling and Ken Pierce and Matt Gregory for assistance with PRR calculations.

References

Armesto, J.J., Pickett, S.T.A., 1986. Removal experiments to test mechanisms of plant succession in oldfields. Vegetation 66, 85–93.

Beers, T.W., Press, P.E., Wensel, L.C., 1966. Aspect transformation in site productivity research. J. For. 64, 691–692.

Canty, M.J., Nielsen, A.A., Schmidt, M., 2004. Automatic radiometric normalization of multitemporal satellite imagery. Remote Sens. Environ. 91 (3-4), 441–451.

Cleary, B., Greaves, R., Hermann, R., 1978. Regenerating Oregon's Forests: A Guide for the Regeneration Forester. Oregon State University Extension Service, Corvallis, OR, pp. 7–27.

Cohen, W.B., Fiorella, M., Gray, J., Helmer, E., Anderson, K., 1998. An efficient and accurate method for mapping forest clearcuts in the Pacific Northwest using Landsat imagery. Photogram. Eng. Remote Sens. 64, 293–300.

Cohen, W.B., Maiersperger, T.A., Spies, T.A., Oetter, D.R., 2001. Modeling forest cover as continuous variables in a regional context with Thematic Mapper data. Int. J. Remote Sens. 22 (12), 2279–2310.

Cohen, W.B., Spies, T.A., Alig, R.J., Oetter, D.R., Maiersperger, T.K., Fiorella, M., 2002. Characterizing 23 years (1972–1995) of stand replacement disturbance in western Oregon forests with Landsat imagery. Ecosystems 5, 122–137.

Cohen, W.B., Maiersperger, T.K., Gower, S.T., Turner, D.P., 2003. An improved strategy for regression of biophysical variables and Landsat ETM+ data. Remote Sens. Environ. 84, 561–571.

Cohen, W.B., Goward, S.N., 2004. Landsat's role in ecological applications of remote sensing. Bioscience 54 (6), 535–545.

Congalton, R.G., 1991. A review of assessing the accuracy of classification of remotely sensed data. Remote Sens. Environ. 37, 35–46.

Coppin, P., Jonckheere, I., Nackaerts, K., Muys, B., 2004. Digital change detection methods in ecosystem monitoring: a review. Int. J. Remote Sens. 25 (9), 1565–1596.

Crist, E.P., Cicone, R.C., 1984. A physically based transformation of Thematic Mapper data—the TM tasseled cap. IEEE Trans. Geosci. Remote Sens. 22 (3), 256–263.

Daly, C., Neilson, R.P., Phillips, D.L., 1994. A statistical-topographic model for mapping climatological precipitation over mountainous terrain. J. Appl. Meteorol. 33, 140–158.

del Moral, R., Bliss, L.C., 1993. Mechanisms of primary succession: insights resulting from the eruption of Mount St. Helens. In: Begen, M., Fitter, A. (Eds.), Advances in Ecological Research, vol. 24. Academic, London, pp. 1–66.

Fiorella, M., Ripple, W.J., 1993. Determining successional stage of temperate coniferous forests with Landsat satellite data. Photogram. Eng. Remote Sens. 59 (2), 236–239.

Foody, G.M., Palubinskas, G., Lucas, R.M., Curran, P.J., Honzak, M., 1996. Identifying terrestrial carbon sinks: classification of successional stages in regenerating tropical forest from Landsat TM data. Remote Sens. Environ. 55, 205–216.

Friedl, M.A., Brodley, C.E., 1997. Decision tree classification of land cover from remotely sensed data. Remote Sens. Environ. 61, 399–409.

Franklin, J., Dyrness, C., 1988. Natural Vegetation of Oregon and Washington. Oregon State University Press, Corvallis, OR, p. 452.

Franklin, J.F., Spies, T.A., Van Pelt, R.V., Carey, A.B., Thornburgh, D.A., Berg, D.R., Lindenmayer, D.B., Harmon, M.E., Keeton, W.S., Shaw, D.C., Bible, K., Chen, J., 2002. Disturbances and structural development of natural forest ecosystems with silvicultural implications, using Douglas-fir forests as an example. For. Ecol. Manage. 155, 399–423.

Hall, F.G., Botkin, D.B., Strebel, D.E., Woods, K.D., Goetz, S.J., 1991. Large-scale patterns of forest succession as determined by remote sensing. Ecology 72 (2), 628–640.

Halpern, C.B., 1988. Early successional pathways and the resistance and resilience of forest communities. Ecology 69, 1703–1715.

Halpern, C.B., 1989. Early successional patterns of forest species: interactions of life history traits and disturbance. Ecology 70, 704–720.

Halpern, C.B., Franklin, J.F., 1990. Physiognomic development of *Pseudotsuga* forests in relation to initial structure and disturbance intensity. J. Veg. Sci. 1, 475–482.

Hardisky, M.A., Klemas, V., Smart, R.M., 1983. The influence of soil salinity, growth form, and leaf moisture on the spectral radiance of *Spartina alterniflora* canopies. Photogram. Eng. Remote Sens. 49, 77–83.

Healey, S.P., Yang, Z., Cohen, W.B., Pierce, D.J., 2006. Application of two regression-based methods to estimate the effects of partial harvest on forest structure using Landsat data. Remote Sens. Environ. 101, 115–126.

Heger, L., 1968. A method for constructing site-index curves from stem analysis. For. Chron. 21, 11–15.

Horler, D.N., Ahern, F.J., 1986. Forestry information content of Thematic Mapper data. Int. J. Remote Sens. 7 (3), 405–428.

Jakubauskas, M.E., 1996. Thematic Mapper characterization of lodgepole pine seral stages in Yellowstone National Park, USA. Remote Sens. Environ. 56, 118–132.

Jensen, J.R., 1996. Introductory Digital Image Processing: A remote sensing perspective, 2nd ed. Prentice Hall, Englewood Cliffs, NJ, p. 318.

Jin, S., Sader, S.A., 2005. Comparison of time series tasseled cap wetness and the normalized difference moisture index in detecting forest disturbances. Remote Sens. Environ. 94, 364–372.

Joyce, S., Olsson, H., 1999. Long-term forest monitoring with temporal-spectral trajectories from Landsat TM data. In: Remote Sensing and Forest Management Conference Proceedings, Rogow, Poland, June 1–3, 1999, http://rogow99.sggw.waw.pl/03_poster_session/08/.

Landis, J.R., Koch, G.G., 1977. The measurement of observer agreement for categorical data. Biometrics 33, 159–174.

Lawrence, R.L., Ripple, W.J., 1999. Calculating change curves for multi-temporal satellite imagery: Mount St. Helens 1980–1995. Remote Sens. Environ. 67, 309–319.

Lawrence, R.L., Ripple, W.J., 2000. Fifteen years of revegetation of Mount St. Helens: a landscape-scale analysis. Ecology 81, 2742–2752.

Lawrence, R.L., Wright, A., 2001. Rule-based classification systems using classification and regression tree (CART) analysis. Photogram. Eng. Remote Sens. 67 (10), 1137–1142.

Lillesand, T.M., Kiefer, R.W., Chipman, J.W., 2004. Remote Sensing and Image Interpretation, 5th ed. John Wiley & Sons, Hoboken, NJ, p. 753.

Lookingbill, T.R., Urban, D.L., 2005. Gradient analysis, the next generation: towards more plant-relevant explanatory variables. Can. J. For. Res. 35, 1744–1753.

Lucas, R.M., Honzak, M., DO Amaral, I., Curran, P.J., Foody, G.M., 2002. Forest regeneration on abandoned clearances in central Amazonia. Int. J. Remote Sens. 23 (5), 965–988.

Lutz, J.A., Halpern, C.B., 2006. Tree mortality during early forest development: a long-term study of rates, causes and consequences. Ecol. Monogr. 76 (2), 257–275.

Ma, Z., Redmond, R.L., 1995. Tau coefficients for accuracy assessment of classification of remote sensing data. Photogram. Eng. Remote Sens. 61 (4), 435–439.

Miller, D.A., White, R.A., 1998. A conterminous United States multi-layer soil characteristics data set for regional and climate and hydrology modeling. Earth Interact. 2 (2), 1–26.

Myster, R.W., Pickett, S.T.A., 1994. A comparison of rate of succession over 18 years in 10 contrasting old fields. Ecology 75, 387–392.

Nesje, A.M., 1996. Spatial patterns of early forest succession in Lookout Creek basin. M.S. Thesis. Oregon State University, Corvallis, OR, 45 pp.

O'Connell, K.E.B., Acker, S.A., Bruner, H.J., Halpern, C.B., Harmon, M.E., 2007. Carbon dynamics of Douglas-fir forests with different successional rates after timber harvest. Unpublished.

Ohmann, J.L., Gregory, M.J., 2002. Predictive mapping of forest. composition and structure with direct gradient analysis and nearest neighbor imputation in coastal Oregon, USA. Can. J. For. Res. 32, 725–741.

Peterson, U., Nilson, T., 1993. Successional reflectance trajectories in northern temperate forests. Int. J. Remote Sens. 14 (3), 609–613.

Pierce, K.B., Lookingbill, T., Urban, D., 2005. A simple method for estimating potential relative radiation (PRR) for landscape-scale vegetation analysis. Landscape Ecol. 20, 137–147.

Richards, F.J., 1959. A flexible growth function for empirical use. J. Exp. Bot. 10, 290–300.

Rouse, J.W., Haas, R.H., Shell, J.A., Deering, D.W., 1973. Monitoring vegetation systems in the Great Plains with ERTS-1. In: Proceedings to the Third Earth Resources Technology Satellite Symposium, vol. 1. pp. 309–317.

Sabol, D.E., Gillespie, A.R., Adams, J.B., Smith, M.O., Tucker, C.J., 2002. Structural stage in Pacific Northwest forests estimated using simple mixing models of multispectral images. Remote Sens. Environ. 80, 1–16.

Schroeder, T.A., Cohen, W.B., Song, C., Canty, M.J., Yang, Z., 2006. Radiometric correction of multi-temporal Landsat data for characterization of early successional forest patterns in western Oregon. Remote Sens. Environ. 103 (1), 16–26.

Smith, M.O., Ustin, S.L., Adams, J.B., Gillespie, A.R., 1990. Vegetation in deserts. I. A regional measure of abundance from multispectral images. Remote Sens. Environ. 31, 1–26.

Song, C., Schroeder, T.A., Cohen, W.B., 2007. Predicting temperate conifer forest successional stage distributions with multi-temporal Landsat Thematic Mapper Imagery. Remote Sens. Environ. 106, 228–237.

Tappeiner, J.C., Huffman, D., Marshall, D., Spies, T.A., Bailey, J.D., 1997. Density, ages, and growth rates in old-growth and young-growth forests in coastal Oregon. Can. J. Forest Res. 27, 638–648.

USDA Forest Service, 1995. Field instructions for the inventory of western Oregon [1995]–1997, http://www.fs.fed.us/pnw/fia/publications/fieldmanuals.shtml.

Venables, W.N., Ripley, B.D., 1997. Modern Applied Statistics with S-plus, 2nd ed. Springer-Verlag, New York, p. 548.

Vermote, E.F., Tanre, D., Deuze, J.L., Herman, M., Morcrette, J.J., 1997. Second simulation of the satellite signal in the solar spectrum, 6S: an overview. IEEE Trans. Geosci. Remote Sens. 35, 895–934.

Viedma, O., Meliá, J., Segarra, D., García-Haro, J., 1997. Modeling rates of ecosystem recovery after fires by using Landsat TM data. Remote Sens. Environ. 61, 383–398.

Yang, Z., Cohen, W.B., Harmon, M.E., 2005. Modeling early forest succession following clear-cutting in western Oregon. Can. J. For. Res. 35, 1889–1900.